

Zhen Jie Boay

Department of Mechanical Precision Engineering,
Malaysia-Japan International Institute of Technology,
University Technology Malaysia,
Jalan Sultan Yahya Petra,
Kuala Lumpur 54100, Malaysia
e-mail: zhenboay@gmail.com

Shye Yunn Heng

Takasago Singapore Pte. Ltd,
1 Jalan Kilang Timor #08-01,
Pacific Tech Centre, 159303, Singapore
e-mail: shyeyunn@tte-net.com

Yutaka Asako¹

Fellow ASME
Department of Mechanical Precision Engineering,
Malaysia-Japan International Institute of Technology,
University Technology Malaysia,
Jalan Sultan Yahya Petra,
Kuala Lumpur 54100, Malaysia
e-mail: y.asako@utm.my

Lit Ken Tan

Department of Mechanical Precision Engineering,
Malaysia-Japan International Institute of Technology,
University Technology Malaysia,
Jalan Sultan Yahya Petra,
Kuala Lumpur 54100, Malaysia
e-mail: tken@utm.my

Nor Azwadi bin Che Sidik

Department of Mechanical Precision Engineering,
Malaysia-Japan International Institute of Technology,
University Technology, Malaysia,
Jalan Sultan Yahya Petra,
Kuala Lumpur 54100, Malaysia
e-mail: azwadi@utm.my

Application of Superposition Principle for Solving a Nonlinear Energy Equation

A new procedure to solve a nonlinear energy equation using the superposition principle is proposed. As an example of the utilization of this procedure, forced convection in a tube with temperature-dependent fluid properties was considered. The tube wall was maintained at uniform wall heat flux axially that varies with time, and the average fluid temperature at the outlet was calculated. This problem simulates convection heat transfer inside a solar collector tube. In the proposed procedure, the average fluid temperature at the outlet for a single heat pulse was determined for fluid properties evaluated at 15 different temperatures by solving the energy equation numerically assuming constant fluid properties and subsequently applying the superposition principle. The choice of the temperature at which fluid properties were evaluated as an important parameter in the simulation. This temperature was determined by using the inlet and outlet average fluid temperatures at the previous time-step multiplied by a weighting function. The average fluid temperature at the outlet obtained by this procedure was compared with the temperature obtained by solving the nonlinear energy equation using variable properties to determine the predictive accuracy of this procedure. The results for one-day operation of a sunny day with fluid velocity of 0.6 m/s, showed the highest root-mean-square (RMS) error of 0.25 K, and the highest mean absolute deviation (MAD) error of 0.16 K which agreed well with the result obtained by the numerical simulation of the nonlinear problem using variable properties. [DOI: 10.1115/1.4053804]

Keywords: superposition principle, nonlinear problem, temperature response, solar collector tube

Introduction

The fluid temperature at the outlet of a solar collector tube fluctuates with time when the solar radiation fluctuates due to the obstruction by clouds. The prediction of the fluid temperature at the outlet of a solar collector tube based on the measured solar radiation data for a period of one year is required for the assessment of a solar thermal system in the early stage of planning in the areas with fluctuating solar radiation [1]. Therefore, reduction of computing time is required. It is well known that superposition principle is only applicable to linear heat transfer problems [2]. A forced convection heat transfer in a tube is the linear problem when fluid properties can be assumed constant. However, it

becomes a nonlinear when the fluid properties greatly vary with temperature such as in the case of oil or oil-based nanofluid [3].

One way to reduce the computational time is to perform a one-dimensional analysis. Liang et al. [4] developed a one-dimensional fluid flow and heat transfer model to simulate heat transfer in a parabolic solar collector tube and concluded that the result of the one-dimensional model was in good agreement with exact results by the three-dimensional model. Also, the simulated average temperature was in agreement with the experimental data. Padilla et al. [5] proved that the one-dimensional numerical heat transfer analysis of solar parabolic trough collector tube was in good agreement with the experimental data. Zaversky et al. [6] developed a one-dimensional fluid flow and transient model of parabolic trough solar collectors, in which the presented model was validated with experimental data. Using one-dimensional commercial software (e.g., MODELICA [7]), the fluid temperature at the outlet of the tube can be obtained. However, such a one-dimensional analysis requires an appropriate estimation for

¹Corresponding author.

Contributed by the Heat Transfer Division of ASME for publication in the JOURNAL OF HEAT TRANSFER. Manuscript received October 11, 2021; final manuscript received February 2, 2022; published online March 4, 2022. Assoc. Editor: Amit Agrawal.

the thermal conductance from the tube wall to the fluid. The accuracy of the simulation results depends on the estimated thermal conductance. However, the thermal conductance between the tube walls to the fluid is not required if the superposition principle can be able to this kind of nonlinear problem since a solution obtained by solving two- or three- dimensional governing equations is superimposed.

Heng et al. [1,8] proposed a combined procedure using artificial neural network (ANN) and superposition principle to solve a nonlinear problem for reduction of the computational time. The proposed procedure was applied for the prediction of the average fluid temperature at the outlet of a parabolic trough solar collector tube whose fluid properties vary with temperature. However, the maximum MAD during one-day operation of the typical sunny days was 2.43 K. The predicted fluid temperature was not very accurate. This motivated the present study to solve the nonlinear energy equation by applying only the superposition principle. In this paper, a new procedure to solve nonlinear energy equations using the superposition principle is proposed. As an example of the utilization of this procedure, the average fluid temperature at the outlet of a tube maintained at constant wall heat flux axially but variable with time was obtained. The numerical results by the proposed procedure were compared with the results obtained considering variable fluid properties and solving the nonlinear heat transfer problem numerically.

Procedure Using Superposition Principle

Description of Example Problem and Governing Equations.

Schematic diagram of the problem under consideration is depicted in Fig. 1. It is the model of a solar collector tube. It is assumed that the outer surface of the solar collector tube is heated with the concentrated heat flux of $\dot{q}(t)$. The concentrated heat flux, $\dot{q}(t)$, is assumed to be uniform in both circumferential and axial directions but fluctuates with time. If the flow is assumed to be fully developed turbulent, the velocity component in r -direction is $v = 0$ and the u component in the flow direction can be expressed by the universal velocity profile. A large number of universal velocity profiles have been proposed by many researchers. The simplest one is the universal velocity profile by Prandtl-Taylor (e.g., Ref. [9]) that is expressed by

$$\begin{aligned} u^+ &= y^+ & (y^+ < 11.6) \\ u^+ &= 2.5 \ln(y^+) + 5.5 & (y^+ \geq 11.6) \end{aligned} \quad (1)$$

where u^+ and y^+ are the dimensionless velocity and the dimensionless coordinate, respectively, and they are expressed as

$$u^+ = \frac{u}{\sqrt{\tau_w/\rho}} \quad y^+ = \frac{y\sqrt{\tau_w/\rho}}{\nu} \quad (2)$$

τ_w is the wall shear stress on the wall and y is a distance from the wall, $y = (D_i/2) - r$. Since $Re = u_{ave}^+(2r_0^+)$ and $u_{ave}^+ = \int_0^{r_0^+} u^+ r^+ dr^+ / \int_0^{r_0^+} r^+ dr^+$, there is the following correlation among the Reynolds number, y^+ and u^+ as [10]

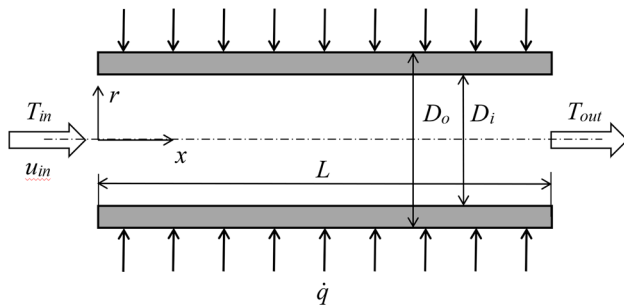


Fig. 1 Schematic diagram of a solar collector tube

$$Re = 4 \int_0^{r_0^+} u^+ dy^+ - \frac{4}{r_0^+} \int_0^{r_0^+} y^+ u^+ dy^+ \quad (3)$$

where $r_0^+ = \frac{(D_i/2)\sqrt{\tau_w/\rho}}{\nu}$.

Substituting Eq. (1) into Eq. (3), then we obtain

$$Re = -154.4 - \frac{711.6}{r_0^+} + 5 r_0^+ \ln(r_0^+) + 3.5 r_0^+ \quad (4)$$

The velocity component, u can be expressed by the universal velocity profile as

$$\begin{aligned} \frac{u}{u_{ave}} &= 4 \frac{(r_0^+)^2}{Re} \left[0.5 - \frac{r}{D_i/2} \right] & (y^+ < 11.6) \\ \frac{u}{u_{ave}} &= \frac{r_0^+}{Re} \left\{ 5 \ln \left(2 r_0^+ \left[0.5 - \frac{r}{D_i/2} \right] \right) + 11 \right\} & (y^+ \geq 11.6) \end{aligned} \quad (5)$$

where u_{ave} is the averaged velocity of the cross-sectional area in the solar collector tube and is obtained from

$$u_{ave} = \frac{\rho_{in}}{\rho_{ave}} u_{in} \quad (6)$$

The velocity profile in the cross-sectional area can be calculated from Eqs. (5) and (6).

The energy equation for fully developed turbulent flow is expressed by

$$\begin{aligned} \rho C_p \frac{\partial T}{\partial t} + \rho C_p u \frac{\partial T}{\partial x} &= \frac{\partial}{\partial x} \left\{ \left(k + \frac{\mu_t}{Pr_t} \right) \frac{\partial T}{\partial x} \right\} \\ &+ \frac{1}{r} \frac{\partial}{\partial r} \left\{ \left(k + \frac{\mu_t}{Pr_t} \right) r \frac{\partial T}{\partial r} \right\} \end{aligned} \quad (7)$$

where μ_t and Pr_t are the turbulent viscosity and turbulent Prandtl number ($Pr_t = 0.9$). Since constant thermo-physical properties are assumed for the tube wall, the energy equation for the tube wall is expressed as

$$\rho_w C_w \frac{\partial T}{\partial t} = k_w \left\{ \frac{\partial^2 T}{\partial x^2} + \frac{1}{r} \frac{\partial}{\partial r} \left(r \frac{\partial T}{\partial r} \right) \right\} \quad (8)$$

where ρ_w , C_w , and k_w are the density, specific heat, and thermal conductivity of the tube wall. Considering a force balance on the fluid element, the shear stress in the fully developed region is expressed by

$$\tau = \tau_w \frac{r}{D_i/2} \quad \text{and} \quad \tau = (\mu + \mu_t) \frac{du}{dy} \quad (9)$$

From Eqs. (2), (3), and (9), $(\mu + \mu_t)/\mu$ can be expressed as

$$\frac{\mu + \mu_t}{\mu} = \frac{r}{D_i/2} \frac{dy^+}{du^+} \quad (10)$$

The derivative of Eq. (1) in the range of $y^+ \geq 11.6$ is

$$du^+/dy^+ = 2.5/y^+ \quad (11)$$

Substituting Eq. (11) into Eq. (10), we obtain

$$\mu_t = \left\{ \frac{r_0^+}{2.5} \frac{r}{D_i/2} \left(1 - \frac{r}{D_i/2} \right) - 1 \right\} \mu \quad (12)$$

We assume $\mu_t = 0$ in the range of $y^+ < 11.6$, since the region is the viscous sublayer. The average fluid temperature at the outlet of the tube is obtained from the following equation.

$$T_{\text{out}} = \int_0^{D_i/2} (\rho u r T)_{\text{out}} dr / \int_0^{D_i/2} (\rho u r)_{\text{out}} dr \quad (13)$$

Initial and Boundary Conditions. It is assumed that the duct wall and fluid temperatures are maintained at T_{in} for $t < 0$. The tube wall is started to heat with uniform heat flux $\dot{q}(t)$ at $t = 0$. Under this assumption, the initial and boundary condition is expressed by Eq. (14). The Sommerfeld boundary condition for uniform heat flux is assumed at the outflow boundary.

$$\begin{aligned} \text{initial conditions } (t < 0): \quad & u = u_{\text{in}}, T = T_{\text{in}} \\ \text{boundary conditions } (t \geq 0) \\ \text{at the inlet } (x = 0): \quad & u = u_{\text{in}}, T = T_{\text{in}} \\ \text{at the outlet } (x = L): \quad & \partial T / \partial t + \bar{u} (\partial T / \partial x) \\ & = \frac{4}{\rho c_p D_i} \dot{q}(t) \frac{D_o}{D_i} \quad (14) \\ \text{on the inner wall } (r = D_i/2): \quad & u = 0 \\ \text{on the outer wall } (r = D_o/2): \quad & k_w (\partial T / \partial r) = \dot{q}(t) \\ \text{on the symmetric line } (r = 0): \quad & \partial T / \partial r = 0 \end{aligned}$$

Numerical Simulation. The energy equations, Eqs. (7) and (8), were discretized using the control volume-based power-law scheme of Patankar [11] coupled with the velocity profile given by Eqs. (5) and (6), and the turbulent viscosity given by Eq. (12), to obtain the responses of the average fluid temperature at the outlet, T_{out} , for a single heating pulse. The discretized equations are solved by using the line-by-line method. Alternating sweep of TDMA in the x - and r -directions is applied.

Therminol VP-1 [12] is selected for the working fluid since the available temperature range of Therminol VP-1 is large and its properties can be expressed as follows:

$$\begin{aligned} \rho &= 1083.25 - 0.90797T + 0.00078116T^2 - 2.367 \times 10^{-6}T^3 \\ C_p &= 1498 + 2.414T + 5.9591 \times 10^{-3}T^2 - 2.9879 \times 10^{-5}T^3 \\ &\quad + 4.4172 \times 10^8T^4 \\ k &= 0.137747 - 8.194777 \times 10^{-5}T - 1.92257 \times 10^{-7}T^2 \\ &\quad + 2.5034 \times 10^{-11}T^3 - 7.2974 \times 10^{-15}T^4 \\ \mu &= 0.00398833 - 5.98717 \times 10^{-5}T + 4.49762 \times 10^{-7}T^2 \\ &\quad - 1.93583 \times 10^{-9}T^3 + 4.81923 \times 10^{-12}T^4 - 6.44657 \\ &\quad \times 10^{-15}T^5 + 3.58355 \times 10^{-18}T^6 \quad (15) \end{aligned}$$

where T is in Celsius. The density and the specific heat of Therminol VP-1 are plotted in Fig. 2 as a function of temperature. Both density and specific heat vary widely with temperature; therefore, this problem is classified as nonlinear. A commercially available collector tube is Schotte PTR70 [13] The geometric parameters and material of the collector tube were determined from the values of Schotte PTR70. The tube length depends on the plant. The most of the length ranges from 96 to 215 m [14]. The geometric parameters and thermo-physical properties of the collector tube are listed in Table 1. Constant thermo-physical properties are assumed for the tube wall.

Procedure for Utilization of Superposition Principle. If we assume the constant fluid properties, the energy equation becomes

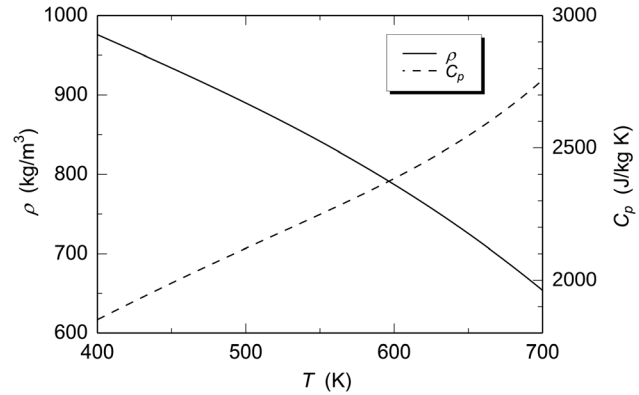


Fig. 2 Density and specific heat of Therminol VP-1

Table 1 Geometric parameters and the thermo-physical properties of the collector tube

Tube length, L	200 m
Outer tube diameter, D_o	0.07 m
Inner tube diameter, D_i	0.065 m
Density, ρ_w	8000 kg/m ³
Specific heat, C_w	500 J/(kg K)
Thermal conductivity, k_w	16.1 W/(m K)

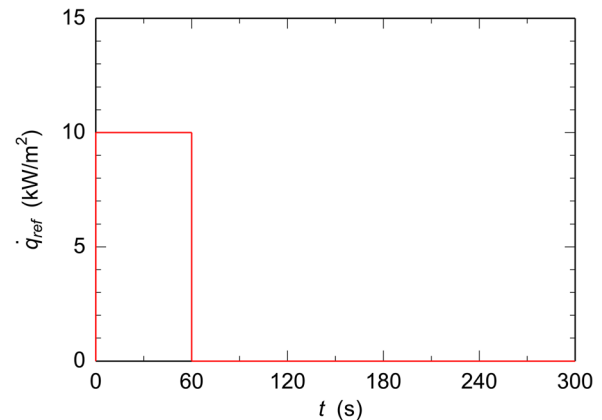


Fig. 3 Single heating pulse

linear and we could apply the superposition principle. Then, the energy equation was solved numerically with the assumption of constant fluid properties to obtain the average fluid temperature at the outlet for a single heating pulse with reference heat flux of $\dot{q}_{\text{ref}} = 10^4$ W/m², with a duration time of $\delta t = 60$ s, and inlet temperature of 413 K. The single heating pulse is plotted in Fig. 3. Any value can be chosen for the reference heat flux, however, a value which is the same order of magnitude as the concentrated heat flux should be chosen to avoid the numerical error. The duration time of the single heating pulse should be equal to that of the heat flux which is calculated from the direct normal irradiance, G_{DNI} , measured every 60 s by Heng [8]. The computations were performed for cases of the fluid properties at 15 different temperatures which range from 413 K to 553 K with an interval of 10 K. The temperature at which fluid property is obtained is called the property temperature in this report. 8 of 15 cases of the temperature increment, $\Delta T = T_{\text{out}} - T_{\text{in}}$, for the single heating pulse and $u_{\text{in}} = 0.35$ m/s are plotted in Fig. 4. These computations were performed with (200×20) grids and the time interval of $\Delta t = 2$ s. The grids were uniformly distributed in the x - and r -directions of the solution domain because the temperature changes in the entire

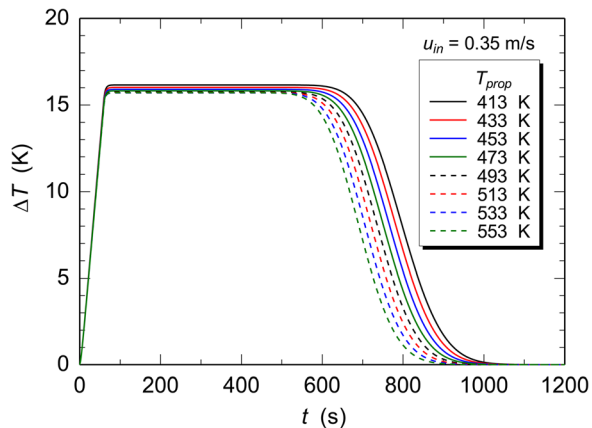


Fig. 4 Response of average fluid temperature at outlet for a single heating pulse ($\dot{q}_{ref} = 10^4 \text{ W/m}^2$)

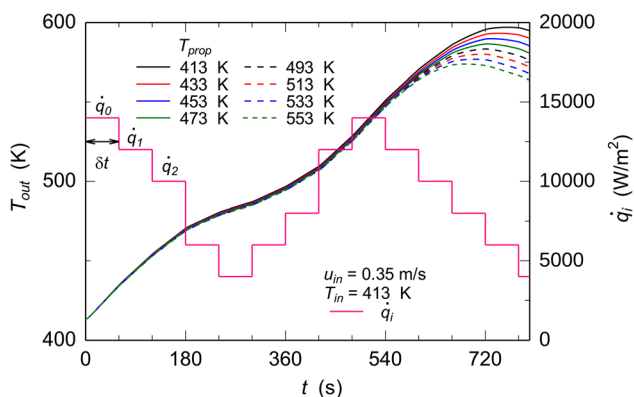


Fig. 5 Example of heating pulses and average fluid temperature at outlet

region of the tube. As the time-step and grid size may affect the results, their effects on the average fluid temperature at the outlet were obtained and will be discussed later.

Subsequently, the superposition principle is applied to obtain the average fluid temperature at the outlet when the tube is heated with heating pulses, \dot{q}_i , as shown in Fig. 5. The temperature increments for the single heating pulse were superimposed. The average fluid temperature at the outlet was calculated from the following equation.

$$T_{out}(t) = \sum_{i=0}^n \Delta T(t - \delta t \times i) \frac{\dot{q}_i}{\dot{q}_{ref}} + T_{in} \quad (16)$$

where δt is the duration time of the single heating pulse. n is the upper limit of summation and it is calculated from $n = \langle t/\delta t \rangle$ where $\langle \rangle$ is a function to cut off below the decimal point. The average fluid temperature at the outlet of the tube was obtained for all cases of the fluid properties at 15 different property temperatures, T_{prop} . 8 of 15 results are also plotted in Fig. 5.

As shown in Fig. 5, the average fluid temperature at the outlet is a function of time and the property temperature, T_{prop} . Therefore, the property temperature is an important parameter in this simulation. In this study, the property temperature T_{prop} was determined from the following equation:

$$T_{prop}(t) = T_{in} \times (1 - w) + T_{out}(t - \Delta t) \times w \quad (17)$$

where w is a weighting factor that is a function of the inlet velocity and $T_{out}(t - \Delta t)$ is the average fluid temperature at the outlet of the previous time-step. Δt is the time-step for solving Eq. (7)

Table 2 Weighting factor, w

Concentrated heat flux $\dot{q}(t) \text{ W/m}^2$	Inlet velocity $u_{in} \text{ m/s}$		
	0.35	0.45	0.60
6,000	0.499	0.5	0.5
8,000	0.5	0.5	0.5
10,000	0.502	0.499	0.499
12,000	0.506	0.501	0.499
14,000	0.513	0.503	0.499

and it is not identical to the heating pulse duration time, δt . Therefore, T_{prop} represents some kind of mean temperature of the fluid in the tube. The weighting factor was determined so that the steady-state average temperatures at the outlet of the tube with constant heat input obtained by the superposition principle coincides with the steady-state average temperature obtained by solving Eq. (7) with variable properties. The weighting factor was obtained for both the heat input range from 6000 to 14000 W/m^2 and the inlet velocity range from 0.35 to 0.6 m/s . The weighting factor is tabulated in Table 2. The weighting factor ranges from 0.499 to 0.513 in this tested range, however, the weighting factor is almost 0.5. Therefore, we used 0.5 for the weighting factor.

As shown in Fig. 5, the average fluid temperature at the outlet, $T_{out}(t)$, were obtained for 15 cases where the fluid properties were evaluated at 15 different property temperatures, T_{prop} , with an interval of 10 K. Therefore, the average fluid temperatures at the outlet, $T_{out}(t)$, is obtained by the linear interpolation as

$$T_{out}(t) = T_{out,L}(t) + \{T_{out,U}(t) - T_{out,L}(t)\} \frac{T_{prop} - T_{prop,L}}{T_{prop,U} - T_{prop,L}} \quad (18)$$

where $T_{prop,U}$ and $T_{prop,L}$ are nearest upper and lower property temperatures. For example, when the property temperature T_{prop} calculated from Eq. (17) is $T_{prop} = 475 \text{ K}$, $T_{prop,U}$ and $T_{prop,L}$ are $T_{prop,U} = 483 \text{ K}$ and $T_{prop,L} = 473 \text{ K}$. $T_{out,U}(t)$ and $T_{out,L}(t)$ are nearest upper and lower outlet temperatures. When the property temperature is $T_{prop} = 475 \text{ K}$, $T_{out,U}$ and $T_{out,L}$ are the average fluid temperatures at the outlet of the tube when the property temperatures are $T_{prop,U} = 483 \text{ K}$ and $T_{prop,L} = 473 \text{ K}$, respectively.

Grid Size and Time Step Effects. As the grid size and the time-step may affect the responses to the average fluid temperature at the outlet, ΔT , supplementary runs were performed to investigate their effects on the ΔT for the single heating pulse. All the computational parameters are identical to those of Fig. 3 with the exception of T_{prop} . T_{prop} was fixed at 493 K. The temperature increment, ΔT , are plotted in Fig. 6 to show the grid size effect. A large discrepancy is observed around $t = 600 \text{ s}$. The grid size effect on the ΔT at $t = 600 \text{ s}$ is tabulated in Table 3. The difference between (400×40) grids and (200×20) grids is minimal. Therefore, (200×20) grids were selected. To show the effect of time-step on ΔT , ΔT are plotted as a function of t in Fig. 7. A large discrepancy is observed around $t = 600 \text{ s}$, too. The time-step effect on the ΔT at $t = 600 \text{ s}$ is tabulated in Table 4. The

Table 3 Grid size effect on ΔT at $t = 600 \text{ s}$ ($u_{in} = 0.35 \text{ m/s}$ and $T_{prop} = 493 \text{ K}$)

Grids	$\Delta t \text{ s}$	ΔT at $t = 600 \text{ s}$	$\frac{\Delta T_{t=600} - \Delta T_{t=600,400 \times 40}}{\Delta T_{t=600,400 \times 40}} \times 100 \%$
50 × 5	2	14.09	-9.3%
100 × 10	2	14.95	-3.8%
200 × 20	2	15.37	-1.1%
400 × 40	2	15.54	—

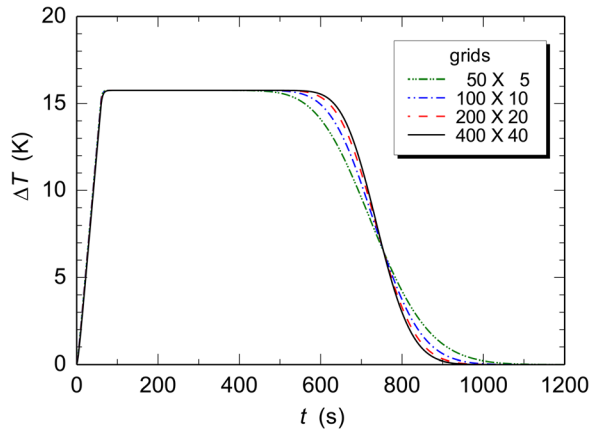


Fig. 6 Grid size effect on ΔT ($u_{in} = 0.35$ m/s and $T_{prop} = 493$ K)

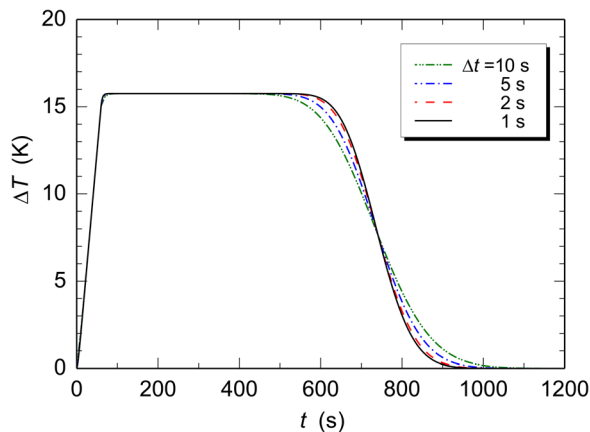


Fig. 7 Effect of time-step on ΔT ($u_{in} = 0.35$ m/s and $T_{prop} = 493$ K)

Table 4 Effect of time-step on ΔT at $t=600$ s ($u_{in} = 0.35$ m/s and $T_{prop} = 493$ K)

Grids	Δt s	ΔT at $t = 600$ s	$\frac{\Delta T_{t=600} - \Delta T_{t=600, \Delta t=1}}{\Delta T_{t=600, \Delta t=1}} \times 100\%$
200 × 20	1	15.51	—
	2	15.37	−0.78 %
	5	14.99	−3.4 %
	10	14.37	−7.4 %

difference between $\Delta t = 1$ s and $\Delta t = 2$ s is slight. Therefore, $\Delta t = 2$ s was selected.

Results and Discussion

The average fluid temperature at the outlet for the case of Fig. 4 obtained by Eq. (18), $T_{out,sup}$ is plotted in Fig. 8 as a function of time. The average fluid temperature at the outlet, $T_{out,variable}$, was also obtained by solving Eq. (7) with variable properties. This result is also plotted in the figure. The MAD, and the root-mean-square error, RMS, between $T_{out,sup}$ and $T_{out,variable}$ were obtained by the following equations.

$$MAD = \frac{1}{N} \sum_{i=1}^N |T_{out,sup} - T_{out,variable}| \quad (19)$$

$$RMS = \sqrt{\frac{1}{N} \sum_{i=1}^N \{T_{out,sup} - T_{out,variable}\}^2}$$

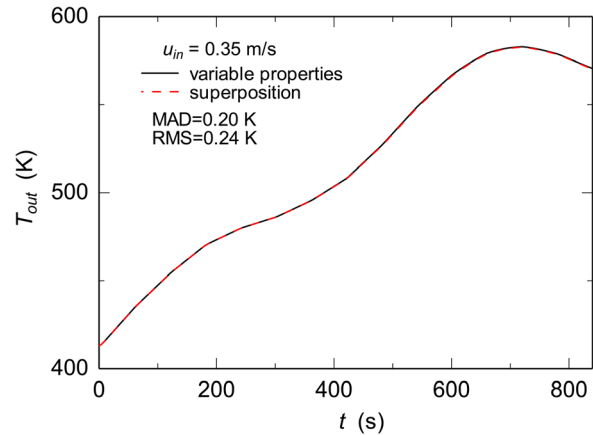


Fig. 8 Average fluid temperatures at outlet for case of Fig. 5

where N is number of dataset. The MAD and RMS of the sample case are 0.20 and 0.24 K, respectively.

A day in equatorial zone countries is classified into a sunny day, a partially cloudy day and a cloudy day by Khatib et al. [15]. The solar radiation in these countries fluctuates and the radiation varies every 1-minute even though it is a sunny day. This section discusses the predictive results of a one-day operation for 11 h from 7 am to 6 pm with a duration time of 60 s ($\delta t = 60$). Figure 9 shows the concentrated heat flux for 30th June, 2018 calculated from the direct normal irradiance, G_{DNI} , measured by Heng [8], which was measured every 60 s. The concentrated heat flux was calculated from [8] as

$$\dot{q}(t) = C_r \times G_{DNI} \quad (20)$$

where C_r is the concentration ratio which was calculated from the mirror concentration ratio of the parabolic trough ($C_m = 82$), the absorptivity of the coated outer surface of the tube ($\alpha = 0.96$) and the effective optical efficiency between the mirror and the outer surface of the tube ($\eta = 0.743$) as

$$C_r = C_m \times \eta \times \alpha / \pi = 18.6 \quad (21)$$

The solar radiation of 30th June 2018 showed a clear sky sunny day in the morning to noon time. Then, large amount of solar

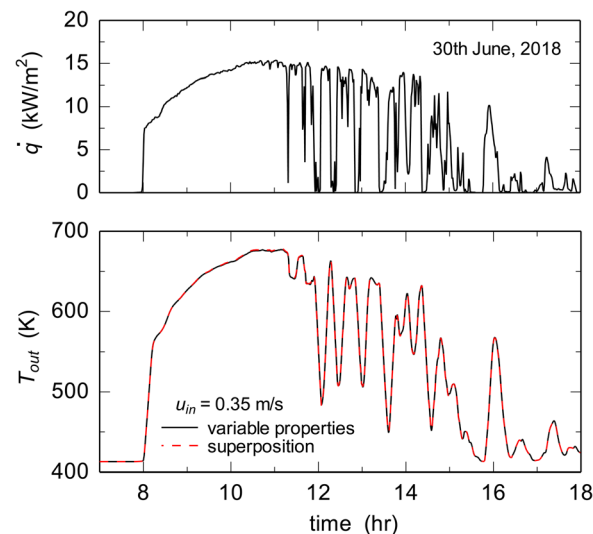


Fig. 9 Concentrated heat flux \dot{q} and T_{out} of partially cloudy day with inlet velocity of 0.35 m/s

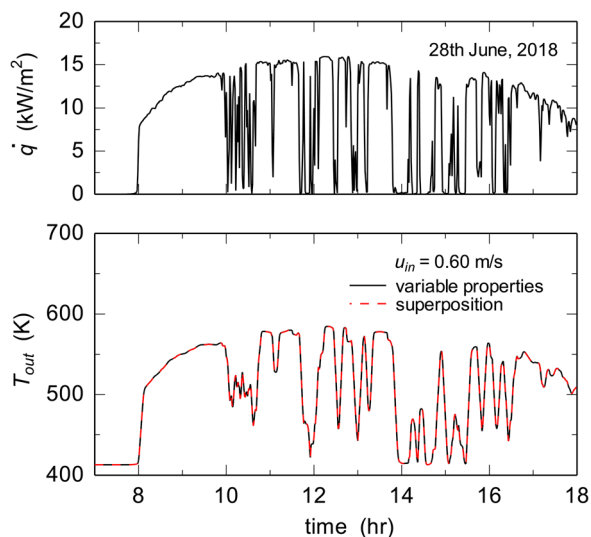


Fig. 10 Concentrated heat flux \dot{q} and T_{out} of sunny day with inlet velocity of 0.6 m/s

fluctuation occurred for the rest of the day by movement of clouds in the sky. The upper value of the fluctuation was reduced. Therefore, 30th June, 2018 was the typical partially cloudy day. The corresponding average fluid temperature at the outlet for a case of $u_{in} = 0.35$ m/s is also plotted in Fig. 9. The prediction using superposition procedure with the heat input of 30th June, 2018 agreed well with the result computed considering variable properties except for 10:30 to 11:30 where the average fluid temperature at the outlet takes the highest. Figure 10 shows the result of 28th June, 2018 of the typical sunny day for a case of $u_{in} = 0.6$ m/s. In this case, the solar radiation fluctuates after 10 am by the clouds. However, the upper value of the concentrated heat flux in each fluctuation is over 10^4 W/m². Therefore, 28th June, 2018 was a typical sunny day. In this case the inlet velocity was high, so the average fluid temperature at the outlet was below 600 K. The prediction using superposition procedure with the heat input of 28th June, 2018 agreed well with the result computed considering variable properties.

The average fluid temperature at the outlet during one-day operation of the typical sunny and partially cloudy days are calculated by the proposed procedure and the MAD, and the root-mean-square error, RMS are obtained. The results are tabulated in Table 5. Values in brackets are the results obtained by the combination procedure of the ANN and the superposition principle [1]. The MADs obtained by the proposed procedures were smaller than MADs obtained by the combination procedure of the ANN and the superposition principle.

It is observed that both RMS and MAD values under higher inlet velocity were low compared to values under lower inlet velocity. The fluid temperature increment between the inlet and

outlet was low when the inlet velocity was high. This is the reason why both RMS and MAD values under higher inlet velocity were low compared to values under lower inlet velocity. Solar radiation fluctuation pattern also affects the RMS and MAD errors. In condition of solar radiation of 14th June 2018, it predicted very well with the lowest error compared to other solar radiation condition. On the other hand, the average fluid temperatures at the outlet on 28th June 2018 and 30th June 2018 were not so well predicted with the higher error among the six chosen days of solar radiation.

The computations were conducted by a personal computer with Intel core i7-4770K 3.50 GHz processor. The proposed method consists of 2 steps. At the first step, the energy equation was solved with the assumption of constant fluid properties to obtain the temperature response (average fluid temperature at the tube exit) for a single heating pulse until $t = 1200$ sec. The computation time (cpu time) for the case of (200×20) grids was 0.969 s. The temperature responses were obtained for 15 cases of the fluid properties at different temperatures. Therefore, the computation time for the first step is 0.969×15 cases = 14.5 s. If the temperature range is wider, more temperature responses are needed. In that case, the computation time for the first step takes more. At the second step, the average fluid temperature at the tube outlet is calculated from Eq. (16). This is the superposition process. The computation time (cpu time) for one-day prediction (11 h) was 1.08 s. The total computation time for one-day prediction was $14.5 + 1.08 = 15.6$ s and the total computation time for one year prediction is 409 s. In contrast, the computation time for the case where the energy equation was solved with the variable properties and (200×20) grids for one day prediction (11 h) was 88.9 s. The computation time for the one-year prediction is 88.9×365 days = 32400 s. The computation time is reduced by applying the proposed method.

Conclusions

A new procedure for solving the nonlinear energy equation using the superposition principle is proposed. As an example of the utilization of this procedure, the average fluid temperature at the outlet of the solar collector tube maintained at uniform wall heat flux axially but variable with time was obtained.

- (1) The proposed procedure improved the accuracy of the prediction of the average fluid temperature at the outlet of the tube. The MAD for the typical sunny day obtained by the combined procedure of the ANN and the superposition principle was 2.43 K, however, the MAD obtained by the proposed procedure was 0.22 K.
- (2) The highest RMS and MAD of the results for the six typical sunny and partially cloudy days obtained by the proposed procedure were 0.84 K and 0.55 K, respectively.
- (3) The computation time of the proposed method for one year prediction including the preparation of the temperature responses is 409 s. In contrast, the computation time for the case where the energy equation was solved with the variable properties and (200×20) grids for the one year

Table 5 Error COMPARISON OF PREDICTION

Date		$u_{in} = 0.35$ m/s		$u_{in} = 0.45$ m/s		$u_{in} = 0.6$ m/s	
		RMS	MAD	RMS	MAD	RMS	MAD
Sunny	180622	0.39	0.23	0.20	0.09	0.12	0.07
	180628	0.84	0.55	0.47	0.27	0.25	0.16 (1.63)
	180719	0.63	0.36	0.38	0.22 (2.43)	0.21	0.12
Partial cloudy	180614	0.36	0.19	0.21	0.11 (1.61 ^a)	0.11	0.06
	180630	0.74	0.47	0.37	0.19	0.19	0.11
	180704	0.38	0.19 (1.62 ^b)	0.21	0.09	0.12	0.06

^aValue obtained for $u_{in} = 0.43$ m/s.

^bValue obtained for $u_{in} = 0.39$ m/s.

prediction is 32400 s. The computation time is reduced by applying the proposed method.

Funding Data

- Takasago Thermal Engineering Co, Ltd., Japan (Grant No: 4B631).

Nomenclature

C_p = specific heat, W/(kg K)
 C_r = concentration ratio
 C_m = mirror concentration ratio
 D_i = inner diameter of solar collector tube, m
 D_o = outer diameter of solar collector tube, m
 \dot{G}_{DNI} = direct normal irradiance, W/m²
 k = thermal conductivity, W/(m K)
 L = length of duct, m
 Pr_t = turbulent Prandtl number
 $\dot{q}(t)$ = concentrated heat flux, W/m²
 r_0^+ = dimensionless radius of duct
 Re = Reynolds number
 t = time, s
 Δt = time step, s
 δt = duration time of single heating pulse, s
 T = temperature, K
 ΔT = temperature increment, K
 u, v = velocity components, m/s
 u^+ = dimensionless velocity
 w = weighting function
 x, r = coordinates, m
 y = distance from wall, m
 y^+ = dimensionless distance from wall

Greek Symbols

α = absorptivity
 η = effective optical efficiency
 μ = viscosity, Pa s
 ρ = density, kg/m³
 τ = shear stress, Pa

Subscripts

ave = cross-sectional average value
 in = inlet

L = lower nearest value
 prop = fluid property
 out = outlet
 ref = reference value
 sup = value obtained by superposition principle
 t = turbulent value
 U = upper nearest value
 variable = value obtained by considering variation of fluid properties
 w = wall

References

- [1] Heng, S. Y., Asako, Y., Suwa, T., and Nagasaka, K., 2019, "Transient Thermal Prediction Methodology for Parabolic Trough Solar Collector Tube Using Artificial Neural Network," *Renewable Energy*, **131**, pp. 168–179.
- [2] Patula, E. J., 1981, "Steady-State Temperature Distribution in a Rotating Roll Subject to Surface Heat Fluxes and Convective Cooling," *ASME J. Heat Transfer-Trans. ASME*, **103**(1), pp. 36–41.
- [3] Mahian, O., Kianifar, A., Kalogirou, S. A., Pop, I., and Wongwises, S., 2013, "A Review of the Applications of Nanofluids in Solar Energy," *Int. J. Heat Mass Transfer*, **57**(2), pp. 582–594.
- [4] Liang, H., You, S., and Zhang, H., 2015, "Comparison of Different Heat Transfer Models for Parabolic Trough Solar Collectors," *Appl. Energy*, **148**, pp. 105–114.
- [5] Padilla, R. V., Demirkaya, G., Goswami, D. Y., Stefanakos, E., and Rahman, M. M., 2011, "Heat Transfer Analysis of Parabolic Trough Solar Receiver," *Appl. Energy*, **88**(12), pp. 5097–5110.
- [6] Zaversky, F., Medina, R., García-Barberena, J., Sánchez, M., and Astrain, D., 2013, "Object-Oriented Modeling for the Transient Performance Simulation of Parabolic Trough Collectors Using Molten Salt as Heat Transfer Fluid," *Sol. Energy*, **95**, pp. 192–215.
- [7] Modelica Association, "The Modelica Association," accessed Jan. 2, 2020, <https://www.modelica.org/>
- [8] Heng, S. Y., 2019, "Thermal Performance Evaluation of Parabolic Trough Collector Tube for Solar Cogeneration System using Artificial Neural Network," Ph.D. thesis, University Technology Malaysia, Malaysia.
- [9] Cengel, Y. A., and Cimbala, J. M., 2010, *Fluid Mechanics*, McGraw-Hill, Inc, New York.
- [10] Asako, Y., and Hong, C., 2017, "Turbulent Temperature Profile in the Quasi-Fully Developed Region of a Micro-Tube," *Bull. JSME, J. Therm. Sci. Technol.*, **12**(1), p. JTST0010.
- [11] Patankar, S. V., 1980, *Numerical Heat Transfer and Fluid Flow*, Hemisphere Publishing Corporation, New York.
- [12] Solutia Inc., 1999, "Heat Transfer Fluid Therminol VP-1," Technical Bulletin 7239115B.
- [13] Schott Solar CSP GmbH, 2013, *SCHOTT PTR@70 Receiver*, The 4th Generation.
- [14] NREL Transforming Energy, Concentrating Solar Power Projects, <https://solarpaces.nrel.gov/>, Dec. 9, 2021.
- [15] Khatib, T., Mohamed, A., Sopian, K., and Mahmoud, M., 2012, "Solar Energy Prediction for Malaysia Using Artificial Neural Networks," *Int. J. Photoenergy*, **2012**, pp. 1–16.